Bone 153 (2021) 116161

Contents lists available at ScienceDirect

Bone

journal homepage: www.elsevier.com/locate/bone

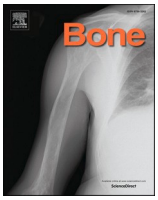

Assessment of the healing of conservatively-treated scaphoid fractures using HR-pQCT

M.S.A.M. Bevers [a,b,c], A.M. Daniels [b,d], B. van Rietbergen [c,e], P.P.M.M. Geusens [f,g], S.M. J. van Kuijk [h], S. Sassen [i], S. Kaarsemaker [j], P.F.W. Hannemann [k], M. Poeze [b,k], H.M.J. Janzing [d], J.P. van den Bergh [a,b,f,g], C.E. Wyers [a,b,f,*]

[a] Department of Internal Medicine, VieCuri Medical Center, Tegelseweg 210, 5912 BL Venlo, the Netherlands
[b] NUTRIM School for Nutrition and Translational Research in Metabolism, Maastricht University Medical Center, P. Debyelaan 25, 6229 HX Maastricht, the Netherlands
[c] Department of Biomedical Engineering, Eindhoven University of Technology, PO Box 513, 5600 MB Eindhoven, the Netherlands
[d] Department of Surgery, VieCuri Medical Center, Tegelseweg 210, 5912 BL Venlo, the Netherlands
[e] Department of Orthopedic Surgery, Maastricht University Medical Center, P. Debyelaan 25, 6229 HX Maastricht, the Netherlands
[f] Department of Internal Medicine, Subdivision of Rheumatology, Maastricht University Medical Center, P. Debyelaan 25, 6229 HX Maastricht, the Netherlands
[g] Department of Medicine and Life Sciences, Hasselt University, Agoralaan 1, 3590 Hasselt, Belgium
[h] Department of Clinical Epidemiology and Medical Technology Assessment, Maastricht University Medical Center, P. Debyelaan 25, 6229 HX Maastricht, the Netherlands
[i] Department of Radiology, VieCuri Medical Center, Tegelseweg 210, 5912 BL Venlo, the Netherlands
[j] Department of Orthopedic Surgery, VieCuri Medical Center, Tegelseweg 210, 5912 BL Venlo, the Netherlands
[k] Department of Surgery and Trauma Surgery, Maastricht University Medical Center, P. Debyelaan 25, 6229 HX Maastricht, the Netherlands

ARTICLE INFO

Keywords:
Fracture healing
Scaphoid fracture
HR-pQCT
Bone density
Bone microarchitecture
Micro-finite element analysis

ABSTRACT

Improving the clinical outcome of scaphoid fractures may benefit from adequate monitoring of their healing in order to for example identify complications such as scaphoid nonunion at an early stage and to adjust the treatment strategy accordingly. However, quantitative assessment of the healing process is limited with current imaging modalities. In this study, high-resolution peripheral quantitative computed tomography (HR-pQCT) was used for the first time to assess the changes in bone density, microarchitecture, and strength during the healing of conservatively-treated scaphoid fractures. Thirteen patients with a scaphoid fracture (all confirmed on HR-pQCT and eleven on CT) received an HR-pQCT scan at baseline and three, six, twelve, and 26 weeks after first presentation at the emergency department. Bone mineral density (BMD) and trabecular microarchitecture of the scaphoid bone were quantified, and failure load (FL) was estimated using micro-finite element analysis. Longitudinal changes were evaluated with linear mixed-effects models. Data of two patients were excluded due to surgical intervention after the twelve-week follow-up visit. In the eleven fully evaluable patients, the fracture line became more apparent at 3 weeks. At 6 weeks, individual trabeculae at the fracture region became more difficult to identify and distinguish from neighboring trabeculae, and this phenomenon concerned a larger region around the fracture line at 12 weeks. Quantitative assessment showed that BMD and FL were significantly lower than baseline at all follow-up visits with the largest change from baseline at 6 weeks (−13.6% and − 23.7%, respectively). BMD remained unchanged thereafter, while FL increased. Trabecular thickness decreased significantly from baseline at three (−3.9%), six (−6.7%), and twelve (−4.4%) weeks and trabecular number at six (−4.5%), twelve (−7.3%), and 26 (−7.9%) weeks. Trabecular separation was significantly higher than baseline at six (+13.3%), twelve (+19.7%), and 26 (+16.3%) weeks. To conclude, this explorative HR-pQCT study showed a substantial decrease in scaphoid BMD, Tb.Th, and FL during the first 6 weeks of healing of conservatively-treated scaphoid fractures, followed by stabilization or increase in these parameters. At 26 weeks, BMD, trabecular microarchitecture, and FL were not returned to baseline values.

* Corresponding author at: VieCuri Medical Center, Department of Internal Medicine, Tegelseweg 210, 5912 BL Venlo, the Netherlands.
E-mail address: c.wyers@maastrichtuniversity.nl (C.E. Wyers).

https://doi.org/10.1016/j.bone.2021.116161
Received 4 February 2021; Received in revised form 19 August 2021; Accepted 20 August 2021
Available online 27 August 2021

1. Introduction

Scaphoid fractures constitute approximately 60–75% of all carpal fractures and have a relatively high incidence in the young and physically active male population [1–4]. They can have a poor clinical outcome when not adequately diagnosed and treated. Delayed and inaccurate diagnosis and inappropriate treatment are among the factors contributing to scaphoid nonunion [5]. Up to 15% of scaphoid fractures develop into scaphoid nonunion [6,7], which can successively cause scaphoid collapse, carpal malalignment and instability, and wrist osteoarthritis, leading to pain and limited functionality [8,9]. Currently, there is no consensus on optimal treatment for scaphoid nonunion, with strategies including internal fixation with screws, K-wires, or mini plates combined with vascularized or non-vascularized bone grafts from mainly the distal radius, medial femoral condyle, or iliac crest [10]. Minimizing the occurrence of a scaphoid nonunion is thus desired considering the consequent additional treatment, prolonged healing times, and possible long-term complications of poor healing. Adequate monitoring of the healing of a scaphoid fracture may help, *e.g.* by enabling early detection of developing complications such as scaphoid nonunion and adjusting treatment strategy accordingly.

However, the possibility to monitor scaphoid fracture healing and to capture changes during healing is limited with current imaging modalities, as is the knowledge regarding the healing process. Today, the monitoring of the healing progress of a scaphoid fracture involves assessment of bone union using for example serial radiography or conventional computed tomography (CT). Radiography is however characterized by a highly subjective evaluation of bone union [11,12]. While conventional CT has been found a reliable and accurate modality to assess scaphoid union and nonunion, assessing partial union is associated with lower interobserver agreement [13], making bone union assessment also on CT partly subjective. Further, radiography and CT cannot provide detailed quantitative information on a microarchitectural level given that their spatial resolution is insufficient to resolve trabecular structures (*e.g.* recently, we used CT with 0.5-mm slice increment for scaphoid fracture diagnosis [14]). Besides that, current knowledge about fracture healing is predominantly based on the healing of diaphyseal fractures that involves mainly cortical bone, while scaphoid fractures concern mainly trabecular bone for which a different healing has been suggested [15–18]. For example, studies on metaphyseal fracture healing in small animals have found that the healing of fractures in trabecular bone is faster and spatially more restricted than fracture healing in cortical bone, and that it resembles direct, intramembranous ossification on surfaces of pre-existing trabeculae and in bone marrow, with little or no cartilage and callus formation [15,16]. A study on knee arthrodeses and more recently on cancellous bone biopsies of fractured distal radii reported similar observations in humans [17,18]. Despite these new insights, detailed and quantitative information about fracture healing of trabecular bone in general and of the scaphoid bone in particular remains limited.

High-resolution peripheral quantitative CT (HR-pQCT) may help to bridge this gap in the monitoring of and knowledge about scaphoid fracture healing as it enables quantitative *in vivo* evaluation of bone on a microarchitectural level. De Jong *et al.* have earlier demonstrated the feasibility of using this imaging modality to quantify the healing process of conservatively-treated distal radius fractures [19,20]. Based on qualitative and quantitative evaluation of HR-pQCT scans of these fractures, they suggested that distal radius fracture healing involves the formation of woven bone that subsequently remodels into a trabecular microarchitecture [19]. Thus far, HR-pQCT has mainly been used for the distal radius or tibia, but recently, we have shown that this imaging modality can also acquire good-quality scans of the scaphoid bone in patients with a suspected scaphoid fracture [21]. Additionally, we have found that HR-pQCT had good interobserver agreement in scaphoid fracture diagnosis and classification [22], and that it revealed 60% more individuals with a scaphoid fracture among 91 patients with a suspected fracture than conventional CT [14]. Besides this benefit to scaphoid fracture diagnosis, HR-pQCT imaging may potentially also be beneficial for the healing of scaphoid fractures by allowing a more detailed and objective healing assessment that could improve the knowledge about scaphoid fracture healing and possibly help to optimize scaphoid fracture treatment. However, the potential to monitor scaphoid fracture healing with HR-pQCT has not yet been investigated. Therefore, the aim of this explorative study was to assess the healing of conservatively-treated scaphoid fractures with HR-pQCT.

2. Materials and methods

2.1. Study design and population

Thirteen patients (8 men, 5 women) aged 18 years and older were included in this prospective cohort study, which was a follow-up of our previously published study in 91 patients (45 men, 46 women) who presented at the emergency department (ED) of VieCuri Medical Center, Venlo (The Netherlands) with a clinically suspected scaphoid fracture. The protocol of this study was approved by an independent Medical Ethics Committee (METC registration number NL62476.068.17). Details about study design, protocol, and population have been earlier described [14,21,22]. Briefly, according to current clinical practice of the hospital, the 91 patients of the main study underwent a standard scaphoid series at first presentation at the ED, followed by wrist immobilization with a polyester cast independent of the diagnosis on the scaphoid series. First presentation at the ED was at the day of trauma in 49 of 91 patients (53.8%) and 1 day after the day of trauma in 29 patients (31.9%). The other 13 patients presented 2–6 days after the day of trauma at the ED. Within 10 days after first presentation, standard physical examination was performed by a trained surgical resident. Additionally, after providing written informed consent, all 91 patients received a baseline CT and HR-pQCT scan at this timepoint. Fracture diagnosis and treatment strategy were based on the evaluation of these two scans. Inclusion criteria to participate in the current follow-up study included a confirmed scaphoid fracture on the baseline HR-pQCT scan and conservative treatment of this fracture with a standard polyester cast. Thirteen patients, who met these criteria, consented to participation in this follow-up study. In eleven of them, the fracture, confirmed on the baseline HR-pQCT scan, was also confirmed on the baseline CT scan, while in the other two patients, the fracture, confirmed on the baseline HR-pQCT scan, could not be confirmed on the baseline CT scan.

2.2. HR-pQCT imaging

HR-pQCT scans were performed of the fractured scaphoid bone at three, six, twelve, and 26 weeks after first presentation at the ED. The scans (XtremeCT II, Scanco Medical AG, Brüttisellen, Switzerland) were acquired using the default clinical *in vivo* settings defined by the manufacturer of the scanner (X-ray tube voltage of 68 kV, intensity of 1460 μA, and integration time of 43 ms). Scan region included a 30.6-mm region of the wrist (three consecutive stacks of 10.2 mm) to cover the entire scaphoid bone (Fig. 1A) [14,21,22]. During acquisition of the scans, the wrist was placed in a standard motion restraining holder while it was immobilized with the polyester cast used for treatment plus an additional single-layer polyester thumb cast (Fig. 1B). The additional thumb cast was used to improve thumb stability [21], and it was only worn during scan acquisition and retained for each scan. After removal of the treatment cast, this cast was also retained for reuse for the remaining scans. Total scan time was six minutes, and the patients were subjected to an effective dose of approximately 15 μSv per scan. The scans were reconstructed with an isotropic voxel size of 61 μm.

The quality of the scans was graded by the operator during scan acquisition based on the grading system originally developed for radius and tibia HR-pQCT scans and constituted inspection of a low-resolution preview of the mid-slice of each stack [23]. Scans were completely

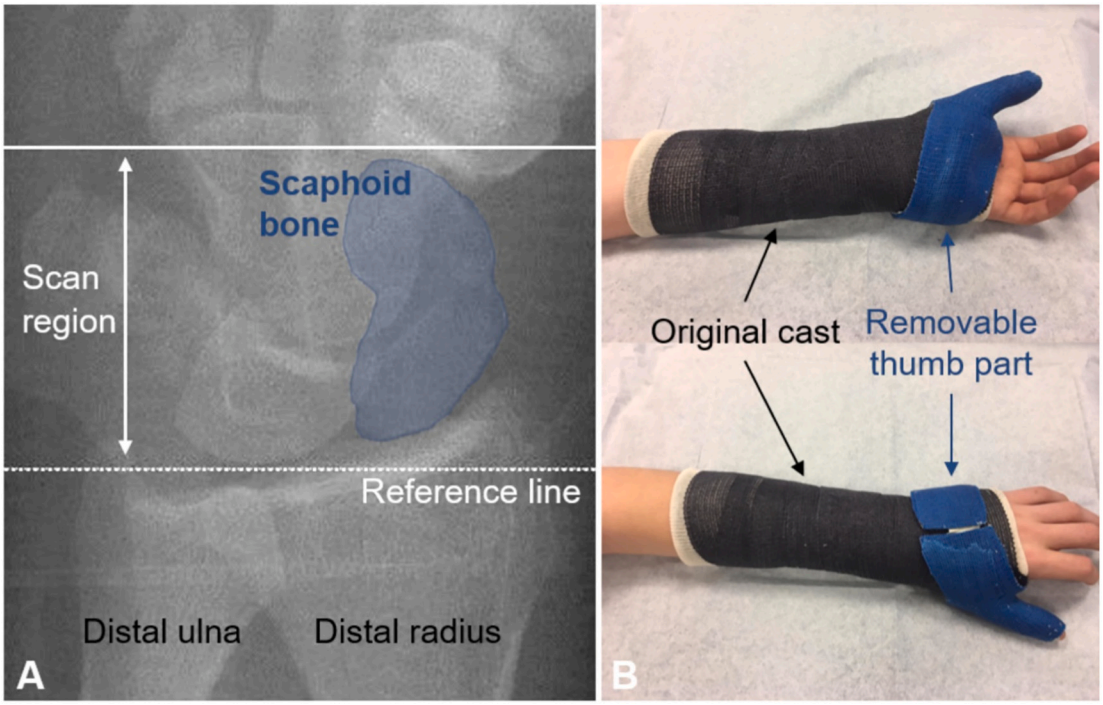

Fig. 1. Example of A) a scout view to define scan region; and B) the polyester cast (black; used for treatment) and removable thumb part (blue; only used during scanning) worn during acquisition of the HR-pQCT scans. (For interpretation of the references to colour in this figure legend, the reader is referred to the web version of this article.)

repeated when the quality of at least one of the three stacks of a scan was graded with a grade > 3 [23]. Only one repetition was allowed, and the scan with the best quality was used for further analyses. In our previously published feasibility study, we reported a considerable discrepancy between the standard grading and a *post hoc* grading [21]. Therefore, the quality of each stack of the scans was *post hoc* graded by one experienced researcher by applying the standard grading system for radius and tibia scans to every tenth full-resolution slice of each stack [21]. Although the scaphoid bone has only a thin outer bone layer compared to the cortex of the distal radius and tibia, motion artefacts in the cortical bone compartment as described in the grading system (*i.e.* horizontal streaking and disruption of the cortical contiguity) could be observed in the outer layer of the scaphoid bone, enabling the use of the standard grading system. The entire scan was assigned a good quality when the three stacks had a *post hoc* grade 1–3 and a poor quality when at least one of the three stacks had a *post hoc* grade > 3.

Previously, we found that a relatively large proportion of scaphoid bone scans (32.9%) had at least one poor-quality stack [21], which could cause a substantial proportion of scans of this study to be excluded. Therefore, justified by the fact that bone parameters are determined over an entire bone volume, it was decided not to exclude all poor-quality scans based on *post hoc* grading to ensure the largest possible dataset for the statistical analyses. To decide which poor-quality scans to exclude, a new grade was assigned to the entire scan by multiplying the *post hoc* grade of each stack with the fraction of the bone volume within that stack (*e.g.* if only 20% of the bone was within the stack, its quality was weighted by 20%). In case the newly determined grade was > 3.5 for the entire scan, the scan was excluded; otherwise, the scan was included. The bone volume of a stack was determined by quantifying the bone volume fraction (BV/TV) of the entire scaphoid bone (*i.e.* including trabecular compartment and outer bone layer) within the stack and subsequently dividing the TV-component of the stack by the TV-component of the entire scan. BV/TV was calculated after standard preprocessing of the scans; that is, after Gaussian filtering with $\sigma = 0.8$ and support = 1 voxel and subsequent bone tissue segmentation with a threshold of 320 mg HA/cm^3.

2.3. Fracture classification

An experienced musculoskeletal radiologist evaluated the HR-pQCT scans at baseline to classify the fractures according to Herbert's scaphoid fracture classification system [24]. Using this system, a scaphoid fracture was classified as stable (type A) or unstable (type B). Stable fractures were further specified as tubercle (A1) or incomplete waist (A2) fractures, and unstable fractures as distal oblique (B1), complete waist (B2) or proximal pole (B3) fractures, transscaphoid perilunate fracture dislocations (B4) or comminuted fractures (B5). The same radiologist also inspected the scans made at 26 weeks to evaluate fracture consolidation by assessing fracture gap bridging and bone remodeling around the fracture region. Consolidation was defined as bridging of the fracture gap with incomplete or complete remodeling of the trabecular bone and outer bone layer.

2.4. Evaluation of bone mineral density and microarchitecture

To allow quantitative evaluation, the scaphoid bones were contoured by application of an automatic contouring algorithm to coarse hand-drawn pre-contours of the scaphoid bone (Fig. 2A) [21]. The coarse pre-contours were drawn to isolate the scaphoid bone from the other bones on the scans [21]. The automatic algorithm, provided by the manufacturer of the scanner, has originally been developed for radius and tibia contouring on HR-pQCT scans and is similar to the automatic contouring algorithm for the peri- and endosteal margins of the radius and tibia on HR-pQCT scans [25]. For application on the pre-contours, the lower threshold to binarize the scans was changed from the default 120 permille (398.2 mg HA/cm^3) to 105 permille (297.7 mg HA/cm^3) to account for the thinner and less mineralized outer layer of the scaphoid bone compared to the cortex of the distal radius and tibia. The resulting contours were manually corrected when visually deviating from the outer bone margins.

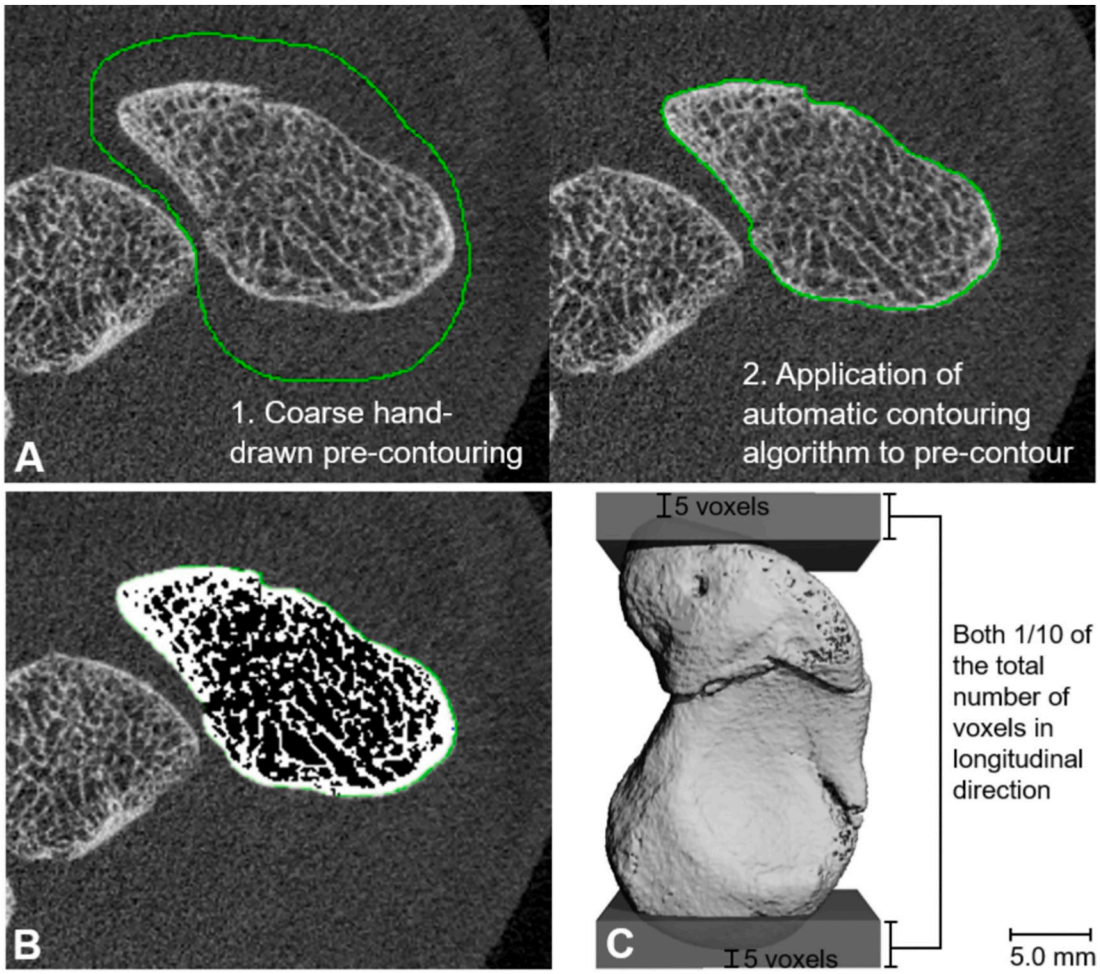

Fig. 2. Example of A) the contouring approach consisting of coarse pre-contouring of the scaphoid bone by hand to isolate it from the other bones (1) and subsequent application of an automatic algorithm to the pre-contour (2); B) the result after pre-processing the scans by Gaussian filtering ($\sigma = 0.8$, support = 1 voxel) and bone tissue segmentation (threshold = 320 mg HA/cm^3); and C) the μFE-approach consisting of alignment of the scaphoid bone along its longest axis and subsequent addition of two stiffer plates at the top and bottom of the scaphoid bone. A compression to 1% strain was applied to the upper plate.

Density and microarchitecture of the contoured scaphoid bones were then quantified using methods based on the standard analysis methods provided by the manufacturer. Conform standard methodology, bone mineral density was calculated directly from the grayscale scans. It was only computed for the entire scaphoid bone (Tt.BMD) and not for the cortical and trabecular compartment. This was done because the thickness of the thin outer bone layer (which is subchondral bone rather than cortical bone) has been found to approximate 1–1.5 times the thickness of an individual trabecula [26], based on which it was chosen to include the outer bone layer in the computation of the trabecular parameters. Consequently, total and trabecular BMD occupied the same bone region, and cortical BMD and cortical microarchitecture were not computed. Besides that, the endocortical contour, standardly determined to separate the cortical and trabecular compartment, was not needed to evaluate trabecular microarchitecture. Instead, the protocol was adjusted so that the obtained outer contour defined the region of interest (*i.e.* the entire scaphoid bone including outer bone layer) from which trabecular microarchitectural parameters were determined. Following the manufacturer's methodology, the scans were first Gaussian filtered ($\sigma = 0.8$, support = 1 voxel) and the bone tissue segmented (threshold = 320 mg HA/cm^3), after which trabecular number (Tb.N), thickness (Tb.Th), and separation (Tb.Sp) were directly measured using the distance transformation method [27]. As all parameters were evaluated for the entire scaphoid bone, no registration was performed between the baseline and follow-up scans. The analyses were performed using the Image Processing Language software provided with the scanner (IPLFE v2.02, Scanco Medical AG, Brüttisellen, Switzerland).

2.5. Evaluation of biomechanical parameters

Micro-finite element (μFE-) modeling was used to estimate the biomechanical properties of the scaphoid bones. As a preprocessing step, the segmented scaphoid bone (obtained from the scan after the filtering and thresholding as explained above) was aligned along its longest axis and placed between two plates (Fig. 2C). For the alignment, the principal axes of the scaphoid bone were determined by calculation of the principal moments of inertia and aligned to the coordinate system of the scan. This step was performed to ensure 1) a consistent loading direction in all patients; and 2) a role for the fracture in all patients independent of fracture type by loading the major part of the bone. A top and bottom plate were successively added to the scaphoid bone in order to prevent unrealistic stress concentrations due to the complex and irregular shape of the bone. These plates were built from isotropic voxels of 61 μm, extended the top and bottom endings of the scaphoid bone with a minimum of five voxels, and both had a thickness of one tenth of the number of voxels in longitudinal direction. The plate voxels attaching to the scaphoid bone were fully bonded to the surface nodes of the bone voxels. The resulting models were converted to μFE-models by conversion of each bone and plate voxel to brick elements of the same size. The

elements constituting the scaphoid bone were assigned a Young's Modulus of 10 GPa and a Poisson's Ratio of 0.3 [28], while those constituting the plates were assigned a ten times higher Young's Modulus (*i.e.* 100 GPa) to mimic material stiffer than bone. An axial compression to 1% strain was then applied in longitudinal direction; that is, the nodes at the top plate were suppressed in the three orthogonal directions, and those at the bottom plate were prescribed a strain of 1 in the longitudinal direction and suppressed in the other two directions. The completed simulations were used to calculate bone stiffness as the reaction force over the applied displacement and to estimate failure load (FL) using Pistoia's criterion [29]. The preprocessing, μFE-model generation, and μFE-analysis were performed using the provided software (IPLFE v2.02).

2.6. Statistical analysis

Statistical analyses were performed in R (R Foundation for Statistical Computing, Version R-3.6.2 for Windows, Vienna, Austria). Linear mixed-effect models (LMMs) were used to model the longitudinal changes in the bone parameters while accounting for clustering of data within patients. Time after first presentation was included as fixed effect and patient identifier as random intercept. Parameter estimation criterion for the LMMs was left as default (*i.e.* restricted maximum likelihood), and no covariates were added to avoid overfitting. The bone parameters at each visit were expressed as estimated marginal means (EMMs) with 95%-confidence intervals, and the significance of the difference of these EMMs between baseline and each follow-up was determined. Also the difference in EMMs between the second follow-up visit and the visits thereafter was determined. The significance level was set at $\alpha = 0.05$ for all tests, and it was not corrected for multiple comparisons due to the small sample size of the study.

3. Results

3.1. Dataset

Eleven of the thirteen included patients completed all five visits (Fig. 3). Two patients did not show up at twelve ($n = 1$) and 26 ($n = 2$) weeks, but the available data of these patients were included in the LMMs. All data of two patients who did complete the follow-up were excluded from the analyses because of surgery after the visit at 12 weeks due to scaphoid nonunion based on follow-up radiographs, CT, and HR-pQCT. One patient with complete follow-up did not wear the additional thumb cast during acquisition of the baseline scan, but the data of this patient could be included in this study based on sufficient image quality. In total, the data of eleven patients were used for the statistical analyses. Baseline characteristics of these patients are presented in Table 1.

Fifty-two HR-pQCT scans were acquired in the eleven patients (Fig. 3). *Post hoc* quality grading revealed fourteen scans (26.9%) with a poor quality in at least one stack due to motion artefacts. Accounting for the relative bone volume affected by the motion artefacts, six HR-pQCT scans (11.5%) remained evaluated as poor quality (Fig. 3) and were excluded from the statistical analyses. The remaining 46 HR-pQCT scans constituted 11 baseline scans, and 9, 10, 7, and 9 scans taken at three, six, twelve, and 26 weeks after first presentation, respectively. The baseline HR-pQCT scan was taken on average 1.3 ± 0.4 weeks after first presentation at the ED and those at the four follow-up visits 3.2 ± 0.5 weeks, 6.1 ± 0.5 weeks, 12.0 ± 1.1 weeks, and 26.0 ± 0.8 weeks after first presentation.

3.2. Visual assessment

Figs. 4 and 5 show examples of the healing of different types of scaphoid fractures. For visualization purposes, the follow-up scans of

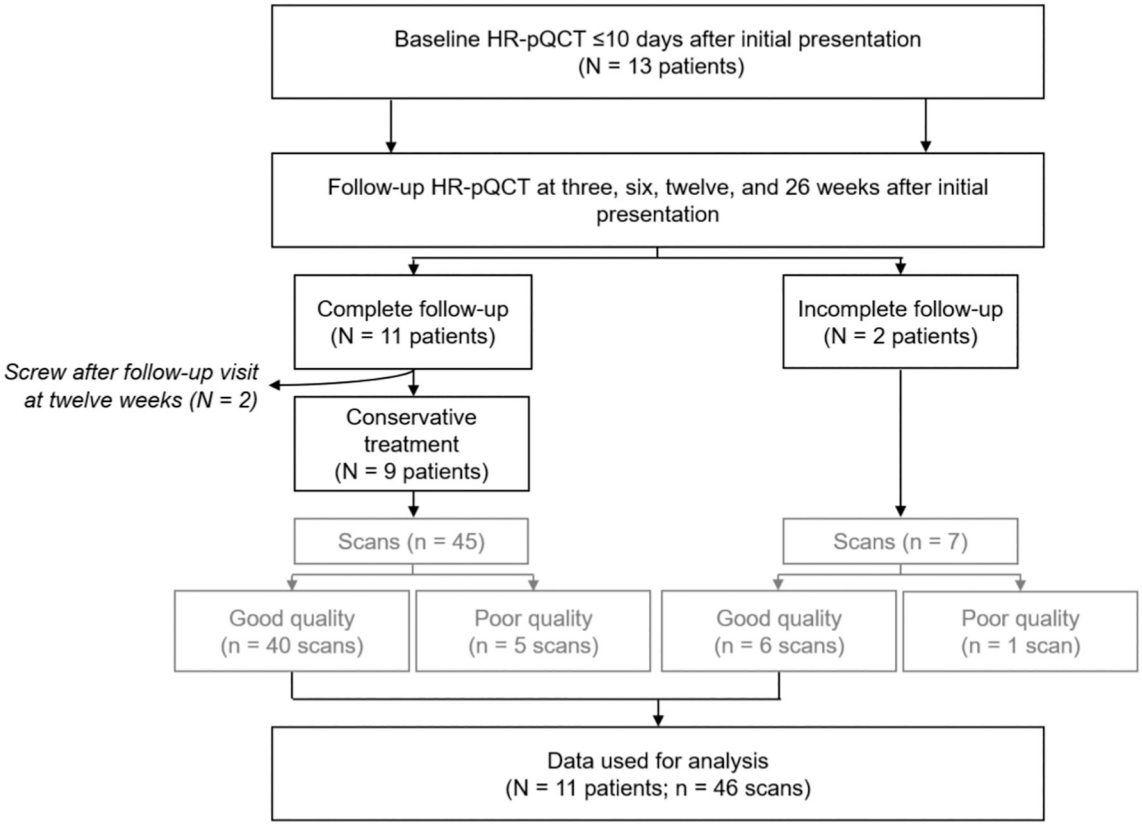

Fig. 3. Flowchart showing the obtained HR-pQCT scans and their quality. Only the scans with a good image quality were used to determine bone mineral density, trabecular microarchitecture, and biomechanical properties of the scaphoid bones.

Table 1
Baseline characteristics of the eleven patients with a scaphoid fracture confirmed on HR-pQCT and treated conservatively whose scans were included in the statistical analyses.

Characteristic	Evaluated patients ($n = 11$)
Male gender	6 (54.5)
Age [years]	47 (19–71, 30)
Initial presentation at the emergency department	
-0 days after the day of trauma (= at day of trauma)	5 (45.5)
-1 day after the day of trauma	3 (27.3)
-2 days after the day of trauma	3 (27.3)
Herbert fracture type (based on HR-pQCT)	
-A1	4 (36.4)
-A2	0 (0.0)
-B1	2 (18.2)
-B2	0 (0.0)
-B3	3 (27.3)
-B4	0 (0.0)
-B5	2 (18.2)
Scaphoid fracture also confirmed on CT	9 (81.8)
Time to cast-removal [weeks]	6.6 (4.7–12.1, 4.3)

Values are expressed as median (minimum-maximum, interquartile range) or frequency (percentage).

these examples were three-dimensionally registered with the baseline scan [30]. In general, the fracture line appeared more pronounced at 3 weeks after first presentation compared to baseline with a disrupted outer bone layer and disrupted trabeculae along the fracture line. Small fracture displacements were observed by visual judgement of one investigator, which might have contributed to a more clearly visible fracture line. At 6 weeks, individual trabeculae at the fracture region became difficult to identify and distinguish from neighboring trabeculae. This 'blurring' of trabecular structures was not visible along the entire fracture line at 6 weeks but became more pronounced and occupied a larger region around the fracture line at 12 weeks (Fig. 5). Finally, at 26 weeks, seven out of the nine fractures with complete follow-up were assessed as consolidated by the radiologist. Two of these seven fractures were assessed as completely bridged but with minor disruptions in the outer bone layer that did not cross the width of the outer layer (*e.g.* Fig. 4; bottom panel). Further, in another consolidated fracture, a small fracture fragment was not fused but got separated. The two other fractures (types B1 and B3) were assessed as nonconsolidated and had small surface and trabecular disruptions (*e.g.* Fig. 4; third panel).

3.3. Quantitative assessment

All parameters except Tb.N had the largest change from baseline at six or 12 weeks, and all but Tb.Th remained significantly different from baseline at 26 weeks (Fig. 6, Table 2). Mean Tt.BMD was significantly lower than baseline throughout the entire follow-up and decreased to the lowest value at six and 12 weeks (−13.6% compared to baseline, both $p < 0.0001$) without significant difference between these timepoints. Tb.Th was significantly different from baseline at three (−3.9%, $p = 0.04$), six (−6.7%, $p = 0.0006$), and twelve (−4.4%, p = 0.04) weeks and was significantly higher at 26 weeks compared to 6 weeks ($p = 0.009$). The other microarchitectural parameters were not significantly different from baseline at 3 weeks but became significantly different thereafter. Tb.N was significantly different from baseline at 6 weeks (−4.5%, $p = 0.01$) and gradually decreased to show the largest difference from baseline at 26 weeks (−7.9%, $p = 0.0001$). Tb.Sp was significantly higher than baseline at six (+13.3%, $p = 0.002$), twelve (+19.7%, p = 0.0001), and 26 (+16.3%, $p = 0.0004$) weeks. The largest percentage changes from baseline were found for the biomechanical parameters with the largest decrease from baseline at 6 weeks (stiffness: −26.5%; FL: −23.7%, both $p < 0.0001$). Thereafter, they increased to a significant difference at 26 weeks compared to 6 weeks (stiffness: $p = 0.0005$; FL: p = 0.0004) but remained significantly lower than baseline (stiffness: −10.9%, p = 0.009; FL: −9.5%, p = 0.01).

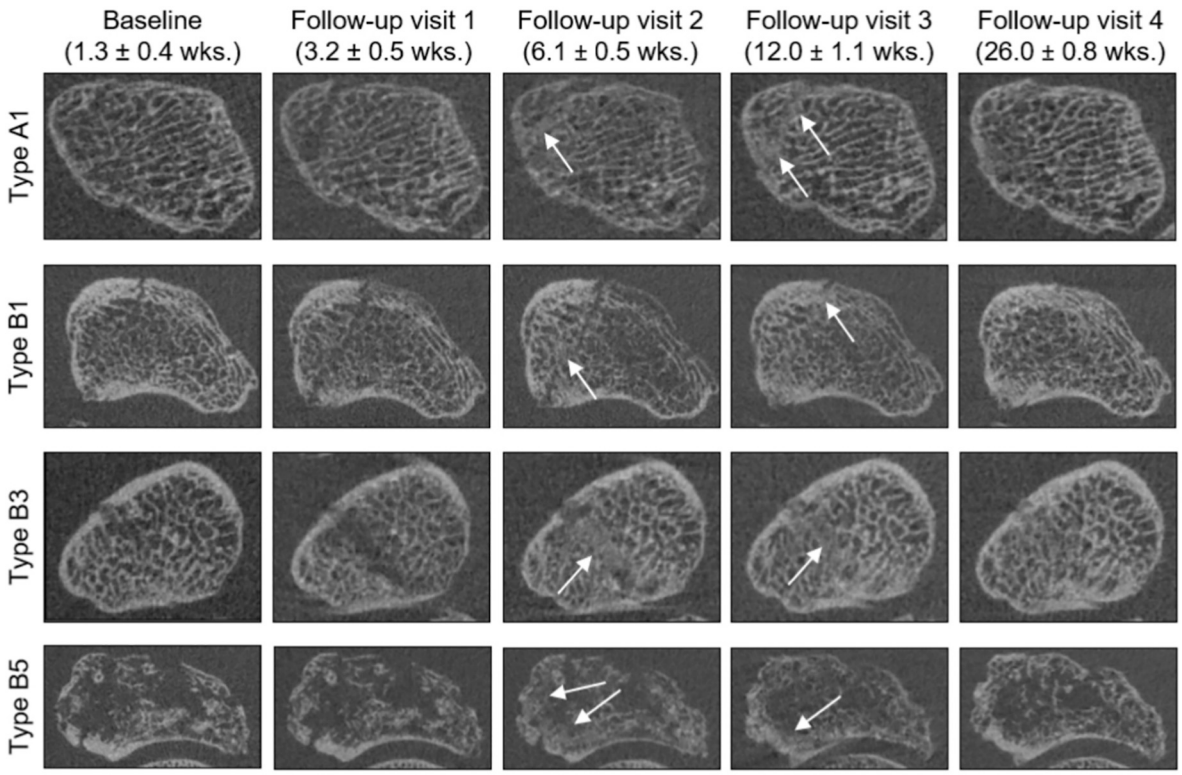

Fig. 4. Examples of HR-pQCT slices of four different types of scaphoid fractures at baseline (left column) and each of the four follow-up visits. The slices were obtained after three-dimensional registration of the follow-up scans with the baseline scan. The white arrows show 'blurring' of trabecular structures with individual trabeculae becoming less well identifiable and distinguishable from neighboring trabeculae.

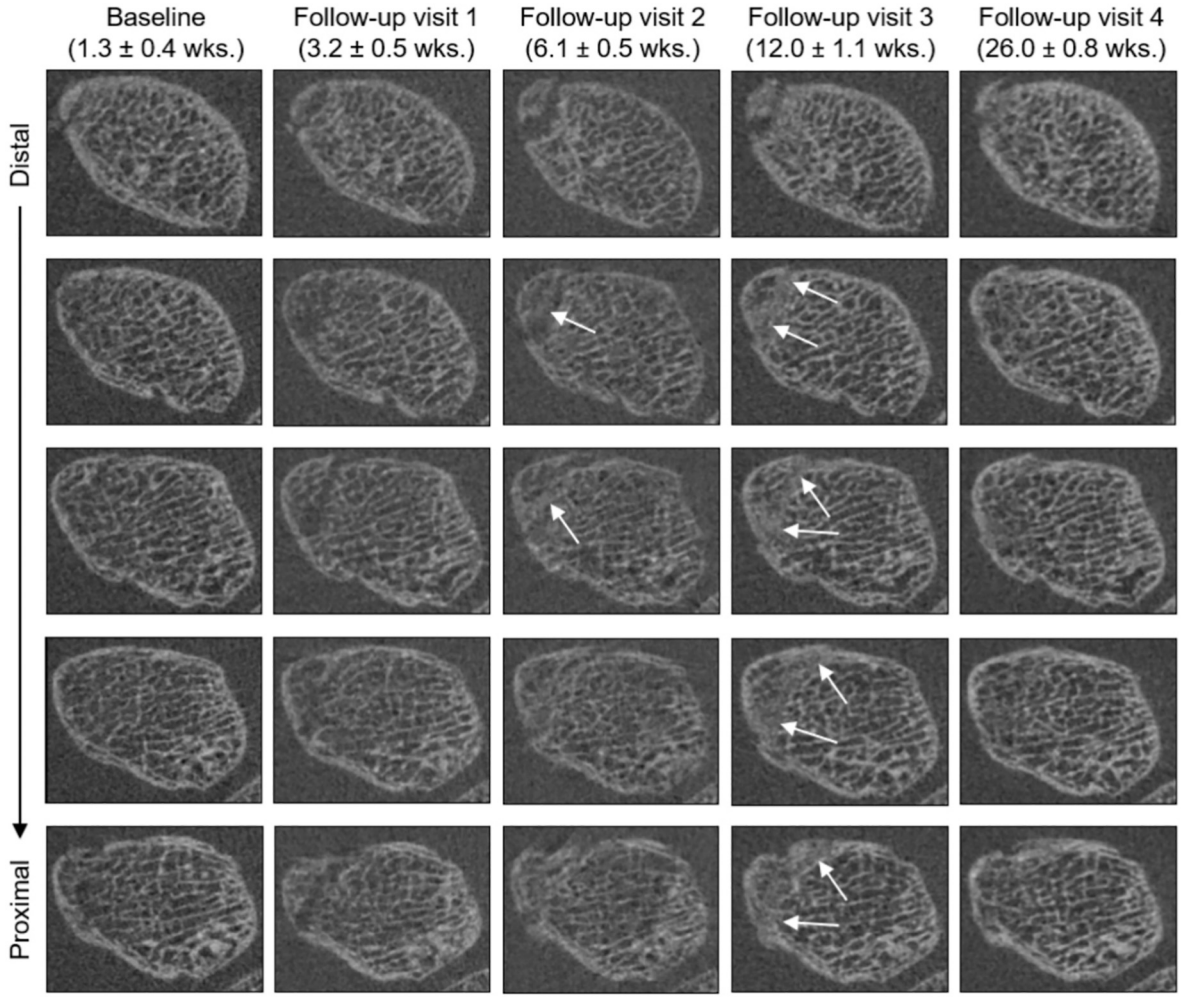

Fig. 5. Multiple HR-pQCT slices of a type A1 scaphoid fracture (shown in Fig. 3; top row) at baseline (left column) and each of the four follow-up visits. The slices were obtained after three-dimensional registration of the follow-up scans with the baseline scan. The white arrows show 'blurring' of trabecular structures with individual trabeculae becoming less well identifiable and distinguishable from neighboring trabeculae.

4. Discussion

This study used for the first time HR-pQCT to explore the healing of conservatively-treated scaphoid fractures. Visual assessment of the HR-pQCT scans revealed an increased fracture visibility at 3 weeks after first presentation at the ED, followed by 'blurring' of trabecular structures around the fracture line at 6 weeks with individual trabeculae becoming hardly indistinguishable from neighboring trabeculae. This 'blurring' became more pronounced at 12 weeks. At 26 weeks, seven out of the nine fractures with complete follow-up were consolidated. Quantitative assessment of the scans showed significant changes in BMD, trabecular microarchitecture, and biomechanical properties of the scaphoid bone during fracture healing with the largest change from baseline at six or 12 weeks for all parameters except Tb.N. At 26 weeks, all parameters except Tb.Th remained significantly different from baseline.

The results may suggest that the healing of the scaphoid fractures assessed in this study consists of two phases. The healing process seemed to be initiated by a significant decrease compared to baseline in BMD, Tb.Th, and stiffness and FL until 6 weeks after first presentation (first phase), co-occurring with an increased visibility of the fracture line at 3 weeks after first presentation. Decreases in areal BMD, assessed with dual-energy X-ray absorptiometry (DXA), have previously been reported five to 10 weeks after first presentation compared to baseline in the proximal and distal part of the scaphoid bone in sixteen individuals with a conservatively-treated scaphoid waist fracture [31]. In that study, decreases in BMD were also found in the ipsilateral uninjured distal radius, and the authors hypothesized that part of the bone loss in the scaphoid bone during fracture healing could be the result of wrist immobilization [31]. Bone resorption has also been reported in a case series on nondisplaced scaphoid fractures using CT five to 7 weeks post-fracture [32]. The assessed fractures healed without surgical intervention, and the authors suggested that bone resorption may be part of the normal scaphoid fracture healing process [32]. Changes in the scaphoid bone during scaphoid fracture healing may thus be the result of a complex multifactorial process. Consequently, the observed initial decrease in total scaphoid BMD could be a result of the actual fracture healing process and of wrist immobilization but possibly also of trauma-induced bone atrophy and reduced blood supply due to a (partially) disrupted vascular network. Also small fracture displacements could have contributed to the decrease in BMD.

During the subsequent phase at twelve and 26 weeks after first presentation, BMD, Tb.Th, stiffness, and FL did not further decrease but stabilized or increased. Nevertheless, all parameters except Tb.Th remained significantly different from baseline at 26 weeks after first presentation. The reduced BMD compared to baseline at 12 weeks agrees with the above-mentioned case series that reported continued resorption in two out of the five patients nine to 16 weeks post-fracture [32]. Combined with the considerable changes between twelve and 26 weeks, our findings suggest that the healing of scaphoid fractures is a slow process that takes months after cast removal and is not completed at 26

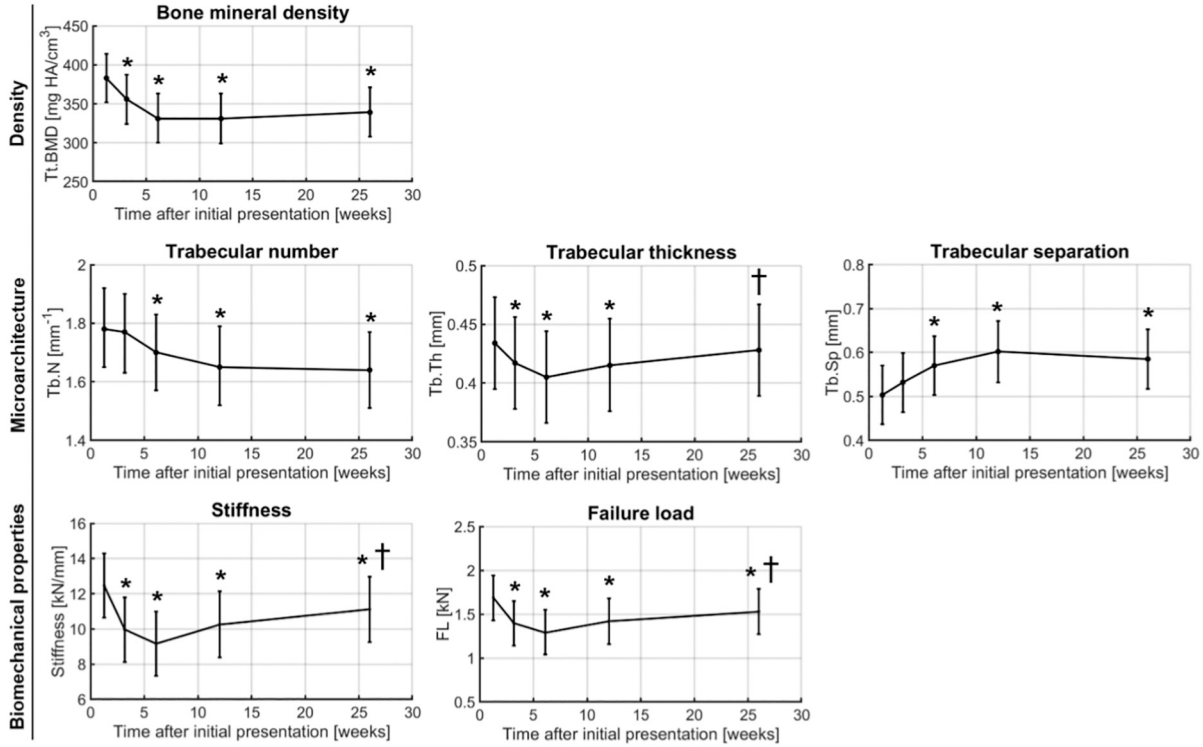

Fig. 6. Time course of the estimated marginal means of bone mineral density (top row), trabecular microarchitecture (middle row), and biomechanical properties (bottom row) of the scaphoid bone obtained from linear mixed effect models with time after first presentation at the emergency department as fixed effect. The error bars show 95%-confidence intervals; * denotes statistically significant differences from baseline and † denotes statistically significant differences at twelve and 26 weeks from 6 weeks (both $p < 0.05$; not adjusted for multiple comparisons).

Table 2
Estimated marginal means (EMMs) of the measured bone parameters at baseline and each follow-up visit with 95%-confidence intervals (95% CI) and percentage change from baseline (n = 11 patients).

Parameter	Baseline (1.3 ± 0.4 weeks after first presentation)	Follow-up visit 1 (3.2 ± 0.5 weeks after first presentation)		Follow-up visit 2 (6.1 ± 0.5 weeks after first presentation)		Follow-up visit 3 (12.0 ± 1.1 weeks after first presentation)		Follow-up visit 4 (26.0 ± 0.8 weeks after first presentation)	
	EMM (95% CI)	EMM (95% CI)	Change from BL (%)	EMM (95% CI)	Change from BL (%)	EMM (95% CI)	Change from BL (%)	EMM (95% CI)	Change from BL (%)
Densitometric									
Tt.BMD [mg HA/cm^3]	383 (352–414)	356 (324–387)*	−7.05	331 (300–363)*	−13.58	331 (299–363)*	−13.58	339 (308–371)*	−11.49
Microarchitectural									
Tb.N [mm^{-1}]	1.78 (1.65–1.92)	1.77 (1.63–1.90)	−0.56	1.70 (1.57–1.83)*	−4.49	1.65 (1.52–1.79)*	−7.30	1.64 (1.51–1.77)*	−7.87
Tb.Th [mm]	0.434 (0.395–0.473)	0.417 (0.378–0.456)*	−3.92	0.405 (0.366–0.444)*	−6.68	0.415 (0.376–0.455)*	−4.38	0.428 (0.389–0.467)†	−1.38
Tb.Sp [mm]	0.503 (0.437–0.570)	0.532 (0.464–0.599)	+5.77	0.570 (0.503–0.637)*	+13.32	0.602 (0.532–0.672)*	+19.68	0.585 (0.517–0.653)*	+16.30
Mechanical									
Stiffness [kN/mm]	12.47 (10.64–14.29)	9.96 (8.11–11.80)*	−20.13	9.17 (7.34–11.00)*	−26.46	10.26 (8.38–12.15)*	−17.72	11.11 (9.26–12.96)*†	−10.91
FL [kN]	1.69 (1.43–1.94)	1.40 (1.14–1.65)*	−17.20	1.29 (1.04–1.55)*	−23.67	1.42 (1.16–1.68)*	−15.98	1.53 (1.27–1.79)*†	−9.47

Tt.BMD = total volumetric bone mineral density; Tb.N = trabecular number; Tb.Th = trabecular thickness; Tb.Sp = trabecular separation; FL = failure load.
Results are obtained from linear mixed effects models with time after first presentation at the emergency department as fixed effect.
Significant differences ($p < 0.05$; not adjusted for multiple comparisons) from baseline are denoted with * and from follow-up visit 2 (for follow-up visits 3 and 4) are denoted with †.

weeks. Physical and radiographical assessment of bone union, on which cast removal is based, seem thus not to coincide with densitometric, microarchitectural, and biomechanical recovery. So, activities of daily life may not require full biomechanical recovery, supporting the clinical advice to increase wrist loading gradually as pain allows after cast removal, as previously also noted in an HR-pQCT study on distal radius fracture healing [20]. Studies have reported significant associations between (changes in) μFE-parameters and (changes in) patient reported pain and function outcome measures during healing in patients with a distal radius fractures [33,34]. Further research is encouraged to investigate the association between biomechanical recovery and functional outcome of scaphoid fractures and to identify whether time to cast

removal could influence biomechanical recovery, which in turn may help to optimize guidelines for conservative treatment strategies for (nondisplaced) scaphoid fractures [35].

Our findings show differences from results of HR-pQCT studies on the healing of conservatively-treated distal radius fractures [19,20]. For example, we observed hardly identifiable and indistinguishable trabeculae around the fracture line at six and 12 weeks, while similar 'blurring' of trabecular structures was seen at already three to 4 weeks in the healing distal radius. Combined with a coinciding increase in trabecular BMD, this observation in the distal radius was earlier suggested to reflect woven bone formation [19]. We did not find a coinciding increase in BMD, but that may among others be due to the subtility of the scaphoid fractures and consequently of the 'blurred' trabecular region, especially when compared to more compressed distal radius fractures. Additionally, we found opposite changes in BMD, Tb.Th, and Tb.Sp, and FL during the first 12 weeks of healing compared to the HR-pQCT studies on distal radius fracture healing. Although our sample size does not allow generalization of the findings, this could imply possible differences in the healing process and timing of scaphoid fractures compared to distal radius fractures. Possible differences could for example be related to the blood supply in the scaphoid bone, which is more tenuous and can be disrupted after fracture [36–38], possibly delaying hematoma formation and inflammation. However, the consequent effects on fracture healing remain to be elucidated as inflammation may play a different role in metaphyseal fracture healing than known from diaphyseal fracture healing [15]. Also, (external) callus formation, found in mechanically unstable distal radius fractures probably from periosteum of the neighboring shaft [15], is less likely in scaphoid fractures due to the predominance of articular cartilage and thus lack of periosteum as well as a limited surrounding space in the wrist [39]. Consequently, excessive inter-fragmentary micromotion due to fracture instability, fracture fragmentation, and finger movements [24,40] may disrupt or delay the formation of osseous bridges between fracture fragments that seems to be important in metaphyseal fracture healing [15]. Future studies on scaphoid fracture healing should investigate the role of vascularity and micromotion on scaphoid fracture healing. Further, they should include a separate analysis of the fractured and intact region of the scaphoid bone including study of bone formation and resorption for varying threshold values in both subregions to investigate changes at the fracture region more detailed as recently done by Atkins *et al.* in distal radius fractures [41]. Additionally, future research should also evaluate the other carpal bones longitudinally, which may provide insights into the possible effects of bone atrophy and wrist immobilization that could impact both scaphoid bone and surrounding carpal bones.

The ability to assess the healing of scaphoid fractures on the microarchitectural level *in vivo* may improve knowledge about the healing process in general and for example the development of scaphoid nonunion in particular. For example, study of the healing of different scaphoid fracture types may provide new insights into the healing process and the timing of healing of the various fracture types and also into possible differences between the types (*e.g.* proximal pole fractures that can be more challenging fractures than other scaphoid fracture types). Such insights could possibly help to optimize treatment strategy for each fracture type. Further, the use of HR-pQCT could improve knowledge about developing scaphoid nonunion and possibly reveal changes in microarchitecture between patients with and without developing nonunion. In an *ex vivo* study using micro-CT, it was earlier reported that bone density and trabecular microarchitecture of the proximal and distal portions of excised scaphoid nonunion specimens were significantly different from the same regions of nonfractured scaphoid bones [42]. In our cohort, two patients had surgical intervention due to suspected nonunion on radiography, CT, and HR-pQCT at 12 weeks, and good-quality scan data of these two patients showed a considerably larger decrease from baseline in Tb.Th at three, six, and 12 weeks compared to the other patients. However, the exploratory design of our study did not allow evaluation of whether early longitudinal changes differed significantly between patients with and without a suspected nonunion and of whether such early changes could possibly help to predict a nonunion, which in turn requires further study.

Despite the novelty of this study, it has several limitations. First, the small dataset did not allow generalization of our findings as well as inclusion of covariates, such as age, gender, and fracture type, in the linear mixed-effects models to explore their influence on fracture healing. Further, we did not adjust for multiple comparisons as that would be at the expense of the power of the study, which was already limited by our sample size. This may increase the risk of type-II errors, but that is acceptable due to the explorative and fundamental nature of this study. Second, the additional thumb cast, only worn during scan acquisition to reduce motion artefacts [21], was not yet used at baseline in one patient, but all data of this patient were included as the thumb cast was single-layered and may thus have had limited effect on radiation absorption and consequently bone parameters. Third, the 'blurring' of trabecular structures around the fracture line at six and 12 weeks could affect the bone parameters as earlier also reported in an HR-pQCT study on distal radius fractures [19] although the amount of 'blurring' and callus was relatively small compared to that observed in the distal radius fractures. To take into account these lower mineralized 'blurred' structures and study the fracture healing in more detail, additional analyses were performed for varying threshold values as suggested by Atkins *et al.* [41] in the entire scaphoid bone. However, these analyses did not reveal new insights compared to using the default threshold value as the relative changes over time were very similar for all chosen thresholds (data not shown). Similarly, fracture size relative to the entire scaphoid bone volume may influence longitudinal changes in BMD and microarchitecture, which are averaged over the entire bone volume, and may have also contributed to the considerable interindividual variation found. We evaluated the bone parameters in the entire scaphoid bone to assess the changes in the entire bone during healing, but as mentioned earlier, further research into scaphoid fracture healing should include separate analysis of the fractured and intact bone region including analysis for multiple threshold values in both subregions [41]. Fourth, the irregular and complex shape of the scaphoid bone challenged μFE-analysis. *In vivo*, scaphoid bones may experience a combination of force and moment components [40]. While the applied force in our simulation may cause a moment component considering the curved shape of the scaphoid bone, *in vivo* loading conditions are more complex. However, although other approaches (*e.g.* other boundary conditions, material properties, or loading directions) may have been possible, and the used Pistoia criterion is not validated for scaphoid bones, the consequent use of one approach and one criterion allowed study of longitudinal changes aimed for. Fifth, due to the novelty of the application, data on the reproducibility of HR-pQCT scanning and contouring of the scaphoid bone are scarce. Recently, we have investigated the interobserver variability of the contouring process. Our results showed that the median of the mean and maximum distance between the contours was 0.004 mm and 0.245 mm, respectively [43]. Further, we reported small but significant differences ($< 1\%$) in density and trabecular microarchitecture between automatic contours without and with manual corrections [21], which might suggest a relatively small effect of correcting the contours. Nevertheless, the influence of motion artefacts and manual contour corrections on bone parameters is unknown and requires future research. Finally, no scans of the contralateral scaphoid bone were available to explore the extent to which the fractured scaphoid bone restored to pre-fracture values, provided that there is bilateral symmetry on the microarchitectural level. Instead, we could only compare with baseline data, which may not well represent pre-fracture values as for example small fractures can already substantially affect biomechanical parameters. It should be considered to include contralateral scans in future HR-pQCT studies on scaphoid fracture healing.

To conclude, HR-pQCT imaging can provide new insights into the healing of scaphoid fractures. In this explorative study, we found that

the healing of the conservatively-treated scaphoid fractures was initiated by significant decreases in bone mineral density, trabecular thickness, and failure load until 6 weeks after first presentation at the emergency department, followed by stabilization or increase of these parameters. Density, bone microarchitecture, and failure load did not return to their baseline values at 26 weeks after first presentation.

CRediT authorship contribution statement

M.S.A.M. Bevers: Conceptualization, Data curation, Formal analysis, Methodology, Writing – original draft, Writing – review & editing, Visualization. **A.M. Daniels:** Data curation, Investigation, Project administration, Resources, Writing – review & editing. **B. van Rietbergen:** Conceptualization, Methodology, Software, Supervision, Writing – original draft, Writing – review & editing. **P.P.M.M. Geusens:** Conceptualization, Supervision, Writing – original draft, Writing – review & editing. **S.M.J. van Kuijk:** Formal analysis, Methodology, Writing – review & editing. **S. Sassen:** Formal analysis, Writing – review & editing. **S. Kaarsemaker:** Resources, Writing – review & editing. **P.F.W. Hannemann:** Validation, Writing – review & editing. **M. Poeze:** Validation, Writing – review & editing. **H.M.J. Janzing:** Conceptualization, Resources, Writing – review & editing. **J.P. van den Bergh:** Conceptualization, Funding acquisition, Supervision, Writing – original draft, Writing – review & editing. **C.E. Wyers:** Conceptualization, Funding acquisition, Project administration, Supervision, Writing – original draft, Writing – review & editing.

Declaration of competing interest

Dr. ir. Bert van Rietbergen is an external consultant for Scanco Medical. All other authors declare that they have no potential conflicts of interest.

Acknowledgements

This work (METC registration number NL62476.068.17) was funded by the research foundation of VieCuri Medical Center Noord-Limburg, The Netherlands.

References

[1] L.M. Hove, Epidemiology of scaphoid fractures in Bergen, Norway, Scand J Plast Reconstr Surg Hand Surg 33 (4) (1999) 423–426.
[2] Van Onselen EBH, R.B. Karim, J.J. Hage, M.J.P.F. Ritt, Prevalence and distribution of hand fractures, J Hand Surg 28 (2003) 491–495.
[3] I. Leslie, R. Dickson, The fractured carpal scaphoid. Natural history and factors influencing outcome, J Bone Joint Surg (Br) 63-B (2) (1981) 225–230.
[4] A.D. Duckworth, P.J. Jenkins, S.A. Aitken, N.D. Clement, C.M. Court-Brown, M. M. McQueen, Scaphoid fracture epidemiology, J Trauma Acute Care Surg 72 (2) (2012), E41.
[5] K. Wong, H.P. Von Schroeder, Delays and poor management of scaphoid fractures: factors contributing to nonunion, J Hand Surg 36 (9) (2011) 1471–1474.
[6] S.L. Filan, T.J. Herbert, Herbert screw fixation of scaphoid fractures, J Bone Joint Surg 78-B (1996) 519–529.
[7] O. Langhoff, J.L. Andersen, Consequences of late immobilization of scaphoid fractures, J Hand Surg 13 (1) (1988) 77–79.
[8] G.R. Mack, M.J. Bosse, R.H. Gelberman, E. Yu, The natural history of scaphoid nonunion, J Bone Joint Surg Am 66 (4) (1984) 504–509.
[9] L.K. Ruby, B.M. Leslie, Wrist arthritis associated with scaphoid nonunion, Hand Clin 3 (4) (1987) 529–539.
[10] R.M. Pinder, M. Brkljac, L. Rix, L. Muir, M. Brewster, Treatment of scaphoid nonunion: a systematic review of the existing evidence, J Hand Surg 40 (9) (2015) 1797–1805.
[11] J.J. Dias, M. Taylor, J. Thompson, I.J. Brenkel, P.J. Gregg, Radiographic signs of union of scaphoid fractures. An analysis of inter-observer agreement and reproducibility, J Bone Joint Surg (Br) 70 (2) (1988) 299–301.
[12] L.A. Hackney, S.D. Dodds, Assessment of scaphoid fracture healing, Curr Rev Musculoskelet Med 4 (1) (2011) 16–22.
[13] P.F.W. Hannemann, L. Brouwers, D. Van der Zee, et al., Multiplanar reconstruction computed tomography for diagnosis of scaphoid waist fracture union: a prospective cohort analysis of accuracy and precision, Skelet Radiol 42 (2013) 1377–1382.
[14] A.M. Daniels, M.S.A.M. Bevers, C.E. Wyers, et al., Improved detection of scaphoid fractures with high resolution peripheral quantitative computed tomography compared to conventional CT, J Bone Joint Surg 102 (24) (2020) 2138–2145.
[15] O.H. Sandberg, P. Aspenberg, Inter-trabecular bone formation: a specific mechanism for healing of cancellous bone: a narrative review, Acta Orthop 87 (5) (2016) 459–465.
[16] S. Inoue, H. Otsuka, J. Takito, M. Nakamura, Decisive differences in the bone repair processes of the metaphysis and diaphysis in young mice, Bone Reports (2018) 81–88.
[17] J. Charnley, S.L. Baker, Compression arthrodesis of the knee: a clinical and histological study, J Bone Joint Surg (Br) 34 (2) (1952) 187–199.
[18] P. Aspenberg, O. Sandberg, Distal radial fractures heal by direct woven bone formation, Acta Orthop 84 (3) (2013) 297–300.
[19] J.J. de Jong, P.C. Willems, J.J. Arts, et al., Assessment of the healing process in distal radius fractures by high resolution peripheral quantitative computed tomography, Bone. 64 (2014) 65–74.
[20] J.J. de Jong, F.L. Heyer, J.J. Arts, et al., Fracture repair in the distal radius in postmenopausal women: a follow-up 2 years postfracture using HRpQCT, JBMR. 31 (5) (2016) 1114–1122.
[21] M.S.A.M. Bevers, A.M. Daniels, C.E. Wyers, et al., The feasibility of high-resolution peripheral quantitative computed tomography (HR-pQCT) in patients with suspected scaphoid fractures, J Clin Densitom 23 (3) (2019) 432–442.
[22] A.M. Daniels, C.E. Wyers, H.M. Janzing, et al., The interobserver reliability of the diagnosis and classification of scaphoid fractures using high-resolution peripheral quantitative CT, Bone Joint J 102 (4) (2020) 478–484.
[23] J.B. Pialat, A.J. Burghardt, M. Sode, T.M. Link, S. Majumdar, Visual grading of motion induced image degradation in high resolution peripheral computed tomography: impact of image quality on measures of bone density and micro-architecture, Bone 50 (1) (2012) 111–118.
[24] T.J. Herbert, W.E. Fisher, Management of the fractured scaphoid using a new bone screw, J Bone Joint Surg (Br) 66 (1) (1984) 114–123.
[25] A.J. Burghardt, H.R. Buie, A. Laib, S. Majumdar, S.K. Boyd, Reproducibility of direct quantitative measures of cortical bone micro-architecture of the distal radius and tibia by HR-pQCT, Bone 47 (3) (2010) 519–528.
[26] A.L. Su-Bum, B.K. Hyo-Jin, C.C. Jae-Myeung, et al., Osseous microarchitecture of the scaphoid: cadaveric study of regional variations and clinical implications, Clin Anat 25 (2) (2012) 203–211.
[27] T. Hildebrand, P. Rüegsegger, A new method for the model-independent assessment of thickness in three-dimensional images, J Microsc 185 (1) (1997) 67–75.
[28] van Rietbergen B, H. Weinans, R. Huiskes, A. Odgaard, A new method to determine trabecular bone elastic properties and loading using micromechanical finite-element models, J Biomech 28 (1) (1995) 69–81.
[29] W. Pistoia, B. van Rietbergen, E.-M. Lochmüller, C.A. Lill, F. Eckstein, P. Rüegsegger, Estimation of distal radius failure load with micro-finite element analysis models based on three-dimensional peripheral quantitative computed tomography images, Bone. 30 (6) (2012) 842–848.
[30] R. Ellouz, R. Chapurlat, B. van Rietbergen, P. Christen, J. Pialat, S. Boutroy, Challenges in longitudinal measurements with HR-pQCT: evaluation of a 3D registration method to improve bone microarchitecture and strength measurement reproducibility, Bone. 63 (2014) 147–157.
[31] N.J. Madeley, A.B. Stephen, N.D. Downing, T.R.C. Davis, Changes in scaphoid bone density after acute fracture, J Hand Surg 31 (4) (2006) 368–370.
[32] S. Fan, N. Suh, R. Grewal, Observation of bony resorption during scaphoid fracture healing: a case series, J Hand Surg Eur 45 (8) (2020) 874–876.
[33] F.L. Heyer, J.J.A. de Jong, P.C. Willems, et al., Long-term functional outcome of distal radius fractures is associated with early post-fracture bone stiffness of the fracture region: an HR-pQCT exploratory study, Bone. 127 (2019) 510–516.
[34] P.J.C. Spanswick, D.E. Whittier, C. Kwong, R. Korley, S.K. Boyd, P.S. Schneider, Improvements in radiographic and clinical assessment of distal radius fracture healing by FE-estimated bone stiffness, Bone Reports 14 (2021) 100748.
[35] M.C. Paulus, J. Braunstein, D. Merenstein, et al., Variability in orthopedic surgeon treatment preferences for nondisplaced scaphoid fractures: a cross-sectional survey, J Orthop 13 (4) (2016) 337–342.
[36] R.H. Gelberman, J. Menon, The vascularity of the scaphoid bone, J Hand Surg 5 (5) (1980) 508–513.
[37] J.S. Panagis, R.H. Gelberman, J. Taleisnik, M. Baumgaertner, The arterial anatomy of the human carpus. Part II: the intraosseous vascularity, J Hand Surg 8 (4) (1983) 375–382.
[38] M. Morsy, M.D. Sabbagh, N.A. van Alphen, A.T. Laungani, A. Kadar, S.L. Moran, The vascular anatomy of the scaphoid: new discoveries using micro-computed tomography imaging, J Hand Surg [Am] 44 (11) (2019) 928–938.
[39] J.F. Slade III, S.D. Dodds, Minimally invasive management of scaphoid nonunions, Clin Orthop Relat Res 445 (2006) 108–119.
[40] J. Erhart, E. Unger, P. Schefzig, et al., In vitro experimental investigation of the forces and torque acting on the scaphoid during light grasp, J Orthop Res 34 (2016) 1734–1742.
[41] P.R. Atkins, K. Stock, N. Ohs, et al., Formation dominates resorption with increasing mineralized density and time postfracture in cortical but not trabecular bone: a longitudinal HRpQCT imaging study in the distal radius, JBMR Plus 5 (6) (2021), e10493.
[42] G. Qu, H.P. Von Schroeder, Trabecular microstructure at the human scaphoid nonunion, J Hand Surg 33 (5) (2008) 650–655.
[43] M.S.A.M. Bevers, C.E. Wyers, A.M. Daniels, et al., Association between bone shape and the presence of a fracture in patients with a clinically suspected scaphoid fracture, J Biomech (2021).